coatings

MDPI

Article

Intrinsic Properties and Future Perspective of $HfO_2/V_2O_5/HfO_2$ Multi-Layer Thin Films via E-Beam Evaporation as a Transparent Heat Mirror

Daniyal Asif Cheema [1,†], Muhammad Osama Danial [1,†], Muhammad Bilal Hanif [2,†], Abdulaziz Salem Alghamdi [3], Mohamed Ramadan [3,4], Abdul Khaliq [3], Abdul Faheem Khan [1,*], Tayyab Subhani [3,*] and Martin Motola [2,*]

1 Department of Materials Science and Engineering, Institute of Space Technology, 1-National Highway, Islamabad 44000, Pakistan; daniyalcheema11@gmail.com (D.A.C.); m.osamadanial030@gmail.com (M.O.D.)
2 Department of Inorganic Chemistry, Faculty of Natural Sciences, Comenius University in Bratislava, Ilkovicova 6, Mlynska Dolina, 842 15 Bratislava, Slovakia; hanif1@uniba.sk
3 College of Engineering, University of Ha'il, Ha'il P.O. Box 2440, Saudi Arabia; a.alghamdi@uoh.edu.sa (A.S.A.); mrnais3@yahoo.com (M.R.); ab.ismail@uoh.edu.sa (A.K.)
4 Central Metallurgical Research and Development Institute (CMRDI), P.O. Box 87, Helwan 11421, Egypt
* Correspondence: afkhan_ist@yahoo.com (A.F.K.); ta.subhani@uoh.edu.sa (T.S.); martin.motola@uniba.sk (M.M.)
† These authors contributed equally to this work.

Abstract: HfO_2 and V_2O_5 as multi-layer thin films are discussed for their potential use as transparent heat mirrors. Multi-layered $HfO_2/V_2O_5/HfO_2$ thin films with a thickness of 100/60/100 nm were prepared via e-beam evaporation on a soda–lime glass substrate. Rutherford backscattering confirmed the multi-layer structure with uniform surface. The as-deposited thin films were annealed at 300 °C and 400 °C, respectively, for 1 h in air. The transmittance of approximately 90% was obtained for all thin films. Due to the relatively low thickness and non-stoichiometry of HfO_2, a band gap of approximately 3.25 eV was determined (instead of the theoretical 5.3–5.7 eV). The as-deposited thin films possessed conductivity of approximately 0.2 $\Omega^{-1}cm^{-1}$ and increased to 1 $\Omega^{-1}cm^{-1}$ and 2 $\Omega^{-1}cm^{-1}$ for thin films annealed at 300 and 400 °C, respectively. Due to the unique intrinsic properties of $HfO_2/V_2O_5/HfO_2$ thin films, the results obtained are promising for application as a transparent heat mirror.

Keywords: V_2O_5; HfO_2; multi-layer; thin films; transparent heat mirror

Citation: Cheema, D.A.; Danial, M.O.; Hanif, M.B.; Alghamdi, A.S.; Ramadan, M.; Khaliq, A.; Khan, A.F.; Subhani, T.; Motola, M. Intrinsic Properties and Future Perspective of $HfO_2/V_2O_5/HfO_2$ Multi-Layer Thin Films via E-Beam Evaporation as a Transparent Heat Mirror. *Coatings* **2022**, *12*, 448. https://doi.org/10.3390/coatings12040448

Academic Editor: Anatoly Kovalev

Received: 20 February 2022
Accepted: 22 March 2022
Published: 25 March 2022

1. Introduction

A pollution-free environment, abundant clean energy, and health risks are the most important challenges of the 21st century. The world is facing harmful consequences due to global warming. As a result of global warming, the use of air conditioners is increasing, leading to increased emission of CO_2 and other carcinogenic atmospheric pollutants that are produced during the electricity generation processes. Major changes are required around us to reduce the effects of global warming [1–5]. For instance, to reduce global warming and energy consumption in buildings, smart windows are promising, as they stop heat radiation. Prolonged exposure to harmful heat radiations (UV and IR) damages the skin and eyes and has an overall negative effect on the quality of living organisms. On a global scale, IR radiation is one of the main sources of global warming. A large amount of energy, which is consumed while lightening a room, is lost through windows. These energy losses could be prevented by improving the thermal performance of windows, thus reducing energy consumption, electricity costs, and emission of greenhouse gases [6–8].

In general, ordinary windows are not able to reflect harmful IR radiation and to transmit VIS radiation; thus, "special" windows are required. On the other hand, Transparent Heat Mirrors (THM) possess the aforementioned properties. Nanostructured multi-layered

THM of suitable composition allow for the transmittance of VIS (λ = 400–700 nm) and reflect IR (λ = 700–3000 nm) from the incident sun rays, providing large energy savings [8]. Due to their high refractive index, the transmission of VIS, reflection of IR, and suitable optical band gap (E_{BG}), HfO_2 (E_{BG} ~5.3–5.7 eV) and V_2O_5 (E_{BG} ~1.7–2.3 eV) are promising for the application of THM [9]. Oxide-based materials play a dominant role in the application of THM due to their promising refractive index. Along with band gap, the refractive index of the materials is an important parameter for determining the efficiency of the materials being used. In the present case, the refractive index of HfO_2 lies in the range of 1.85–2.1, whereas the refractive index of V_2O_5 falls around 2.70, which is very suitable for the application of THM [10,11]. Formally, the dielectric/metal/dielectric structure has been used for THM. However, the second metallic layer (which can be made of silver, molybdenum, gold, aluminum, copper, etc.) in this structure causes reduced transmittance. That is why, in the present research, the metallic layer has been replaced with another metal oxide layer, V_2O_5, due to its attractive optical properties [12,13].

Manufacturing cost, lifetime, weight, and retrofit capability are crucial factors in determining which THM could potentially be suitable for use in public facilities. Indeed, fabrication procedure and materials selection are the main factors that influence the overall applicability of THM. Over the past few years, several techniques have been used to fabricate THM, including Physical Vapor Deposition and Chemical Vapor Deposition. The electron beam (e-beam) evaporation technique provides dense and uniform films but is overlooked in the current field of THM [14–16]. Due to this scientific knowledge gap, we focused our work on the preparation of THM using e-beam evaporation.

In the presented work, a novel material that is suitable for energy-efficient films and is economically affordable was prepared. Multi-layered $HfO_2/V_2O_5/HfO_2$ thin films were prepared via e-beam evaporation with thickness 100/60/100 nm on soda–lime glass for applications in THM. Relatively easy and affordable fabrication of the films would provide cost-effective and efficient windows for future buildings. The presented THM could potentially reduce the emission of greenhouse gases and decrease energy consumption in public facilities.

2. Experimentation

HfO_2 (purity > 99.99%) and V_2O_5 (purity > 99.9%) powders were used as starting materials, which were converted to pellets using polyvinyl gel (PVA) as a binder. Briefly, 2.5 g of PVA gel was dissolved in 100 mL of distilled water. Afterward, the solution (binder) was heated to 200 °C and stirred for 3 h. The binder solution was subsequently used for 10 mm thick pellets, prepared by applying 600 Torr using a hydraulic press.

Tri-layer nanostructure was manufactured by EDWARD vacuum coating system (A306, USA). Pellets of HfO_2 and V_2O_5 were prepared from the powder and were placed in two molybdenum crucibles. Targeted palettes were heated by an electron beam collimated from DC-heated tungsten cathode filament, and the pellets' surfaces were bombarded by a 180° deflected electron beam with accelerating voltage of 3.8 kV. The electron beam was operated at 10–20 kW power. To achieve uniformity of deposited layers, the distance between source and target was 6 cm, and the substrate holder was rotated at 30 rpm. As a result, the evaporated species were deposited on the substrate surface as a nanolayer. Film thickness was measured by a quartz crystal monitor during the entire deposition process. First, the layer of HfO_2 with a thickness of ~100 nm was deposited on a glass substrate (Figure 1a) at a temperature of 270 °C. Subsequently, V_2O_5 (Figure 1b; ~60 nm thickness, 200 °C) and HfO_2 (Figure 1c; ~100 nm thickness, 270 °C) were deposited, respectively.

Different kinds of thin films were fabricated: (i) as-deposited; (ii) annealed at 300 °C; and (iii) annealed at 400 °C. Optical transmittance was measured at room temperature using a Perkin Elmer UV/VIS/NIR Lambda 19 spectrophotometer (USA) at room temperature at the wavelength range from 300 nm to 2500 nm. A (5MeV) Tandem Pelletron Accelerator (5UDH-2 pelletron, National Electrostatics Corporation, Middleton, WI, USA) was used for Rutherford backscattering (RBS) to determine the thickness, elemental composition,

depth profiling, and surface properties of the thin films. The beam of helium particles (He^{2+}; with an average energy of 2 MeV) with Cornell geometry was used to obtain the RBS spectrum and simulated using SIMNRA and XRUMP software (version 6.05), with an incident scattering angle of 170°, by keeping the 13 cm distance between sample and detector. The absorption depth was calculated using absorption coefficient (α) as follows:

$$\text{Absorption depth} = 1/\alpha$$

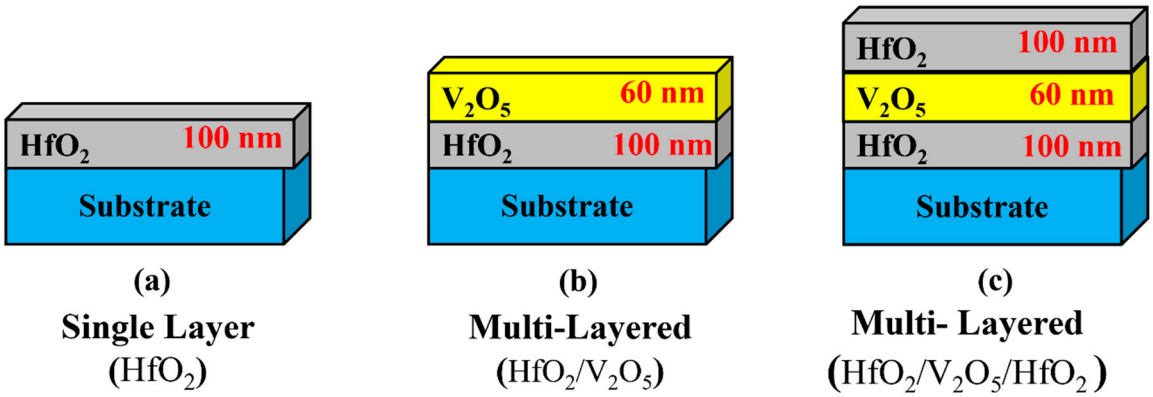

Figure 1. Schematic illustrations of (**a**) HfO_2; (**b**), HfO_2/V_2O_5; and (**c**) $HfO_2/V_2O_5/HfO_2$ thin films.

The conductivity of fabricated thin films was measured via DC-2 probe point tests. The values of length, width, and height of the sample were known; thus, the resistance was calculated by using the formula V = IR.

3. Results

Electron beam evaporation is a very cost-effective technique that can fabricate films at the nanoscale with good accuracy. However, the deposition parameters play a dominant role in determining the thickness and uniformity of the films deposited. In the present research, V_2O_5 and HfO_2 are very tricky materials due to the dissociation of oxygen during deposition, which ultimately causes more non-stoichiometry in the deposited films [17–19]. For these reasons, the deposition parameters were optimized after many trials with good control over thickness. First, we optimized the thicknesses of the different layers, i.e., HfO_2 and V_2O_5, via RBS; the results are summarized in Table 1. Numerous samples were prepared, with different thicknesses of the thin films (from 70 to 4000 nm) and in-depth profiling, along with an elemental analysis conducted to determine the surface quality and stoichiometry of the thin films. This is discussed in more detail later in the manuscript. Based on these preliminary results, the most promising thin films, with a thickness of 100/60/100 nm ($HfO_2/V_2O_5/HfO_2$), were further studied for their potential application as THM.

Table 1. In-depth profiling thickness and the elemental ratio of as-deposited samples.

Layer	Thickness	Hf	V	O (Film)	Si	Ca	O (Substrate)
1	104 nm	0.279	0	0.720	0	0	0
2	104–159 nm	0	0.249	0.750	0	0	0
3	159–255 nm	0.721	0	0.278	0	0	0
4	255–4000 nm	0	0	0	0.336	0.028	0.636

Figure 2 shows the plots of transmittance vs. wavelength of as-deposited multi-layered $HfO_2/V_2O_5/HfO_2$ thin films annealed at 300 °C and 400 °C. The optical transmittance in the visible range reached approximately 90% in all thin films. In thin films annealed at 400 °C, only one peak appeared in the spectrum (Figure 2c). This is due to the increased

annealing temperature where the thin films of HfO_2 and V_2O_5 diffused into each other. Nevertheless, all thin films were highly active in the visible range.

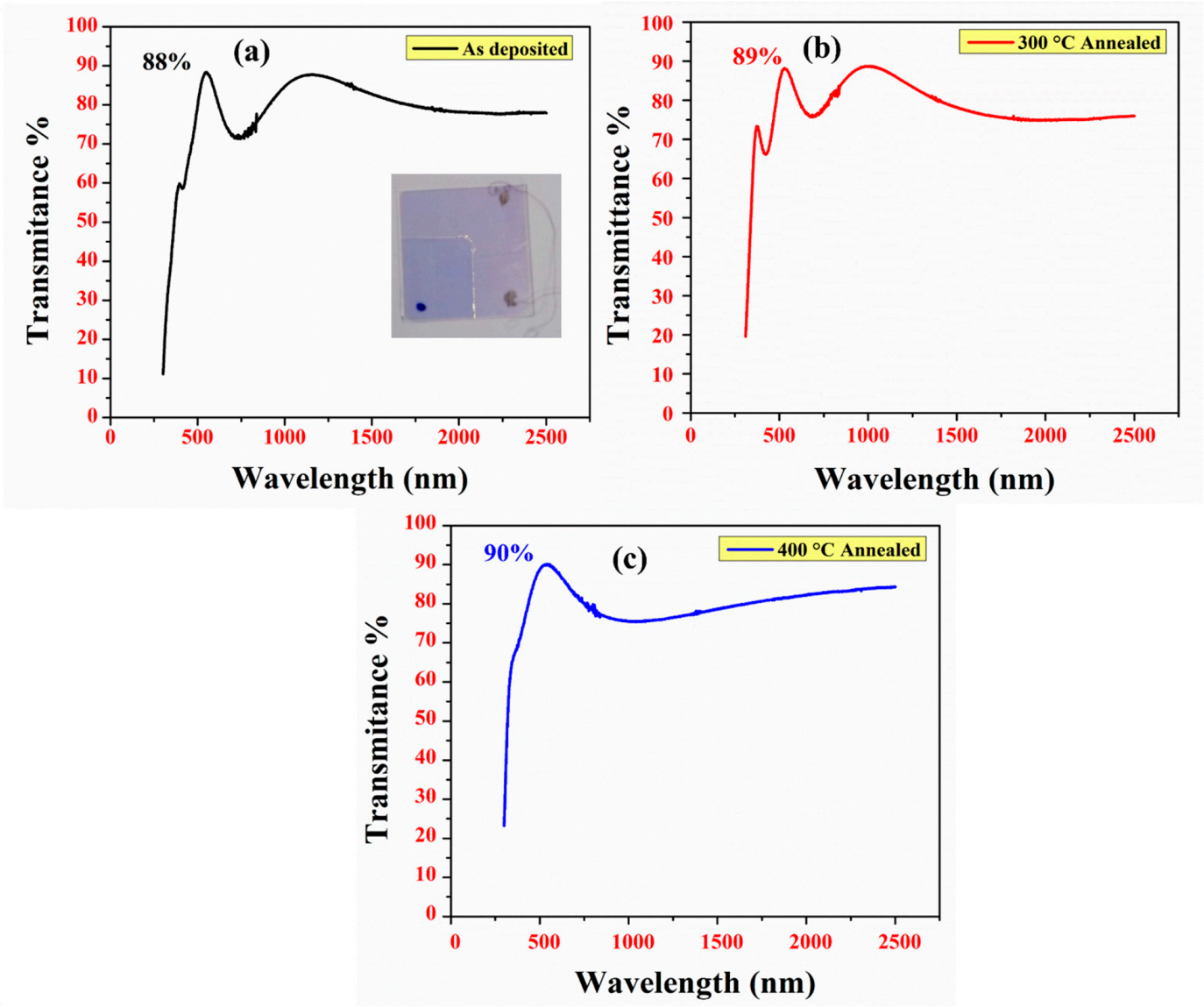

Figure 2. Transmittance spectra of multi-layered $HfO_2/V_2O_5/HfO_2$ thin films: (**a**) as-deposited; (**b**) annealed at 300 °C; (**c**) annealed at 400 °C.

The absorption coefficient (or attenuation coefficient) of the thin films was calculated using the following equation:

$$\alpha = \ln(1/T)/x \quad (1)$$

where α is the absorption coefficient, T (%) is the transmittance, and x (nm) is the thickness of the thin films.

A Tauc plot (Figure 3) was used to calculate the optical band gap by plotting the absorption coefficient vs. photon energy [20,21]. The photon energy was calculated using Equation (3):

$$h\nu = 1240/\lambda \quad (2)$$

where hν (eV) is the photon energy and λ (nm) is the incident wavelength.

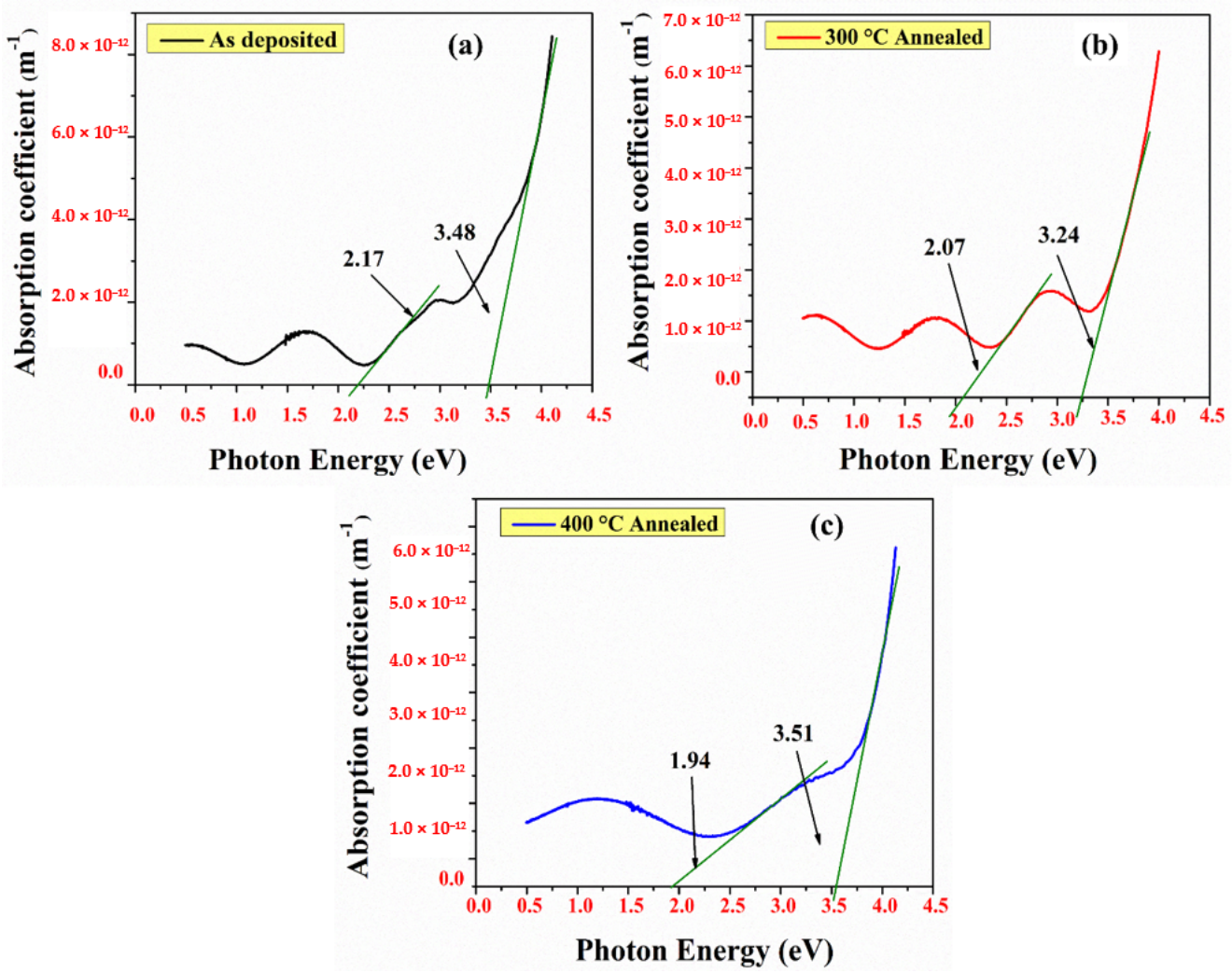

Figure 3. The plot of optical absorption coefficient (α) vs. photon energy (hν) of multi-layered $HfO_2/V_2O_5/HfO_2$ thin films: (**a**) as-deposited; (**b**) annealed at 300 °C; and (**c**) annealed at 400 °C.

Figure 3 shows the optical band energy gap vs. photon energy for the multi-layer thin films. Figure 3a shows two distinct band gap energies for the as-deposited film. The optical band gaps (E_{BG}) of 3.48 eV and 2.17 eV were obtained for the as-deposited HfO_2 and V_2O_5 thin films, respectively. It is clear from Figure 3a that the multi-layer films were deposited with a sharp interface at the nanoscale using an electron beam evaporation technique. A decrease in E_{BG} was observed after annealing at 300 °C (E_{BG} ~3.24 eV HfO_2; E_{BG} ~2.07 eV V_2O_5). This decrease may be attributed to a decrease in defect density, a decrease in residual stresses generated during deposition and structural modifications [22]. At 400 °C, the increase in E_{BG} was observed, with a continuous decrease in band gap of V_2O_5 (E_{BG} ~3.51 eV HfO_2; E_{BG} ~1.94 eV V_2O_5). The results are quite interesting here. At this high temperature, the oxygen from the upper layer of HfO_2 diffused to the second layer (V_2O_5), causing more stoichiometry in the V_2O_5 layer and non-stoichiometry in the HfO_2 layer, which caused the E_{BG} of HfO_2 to rise. The calculated E_{BG} for V_2O_5 agrees with the theoretically calculated values from the literature, i.e., 1.7–2.3 eV. A significant decrease in E_{BG} of HfO_2 was observed compared to the reported E_{BG} values, i.e., 5.3–5.7 eV [23,24]. This is due to the reduced particle size, the relatively low thickness of the films, and the non-stoichiometry of HfO_2. The overall E_{BG} reduction (from as-deposited to annealed thin films) was due to increased annealing temperature. Indeed, increased annealing temperature resulted in enhanced grain growth, structure modification, and porosity reduction in the thin films [25–27].

To confirm the efficient transmittance of the thin films, measurements of absorption depth vs. wavelength of the thin films were conducted and are shown in Figure 4. Absorption depth is basically the measure of penetration of electromagnetic radiations in a particular material before they are absorbed or reflected. In the present samples, the radiation entered the samples and was reflected back in the visible range of the solar spectrum, as shown in Figure 4. However, the films annealed at 400 °C (Figure 4c) showed better results than all radiation other than visible light reflected in the near IR region. All in all, the obtained results from the optical characterizations (Figures 2–4) of the thin films were all in agreement. The prepared thin films possessed the optical properties crucial for the application of the presented material as THM.

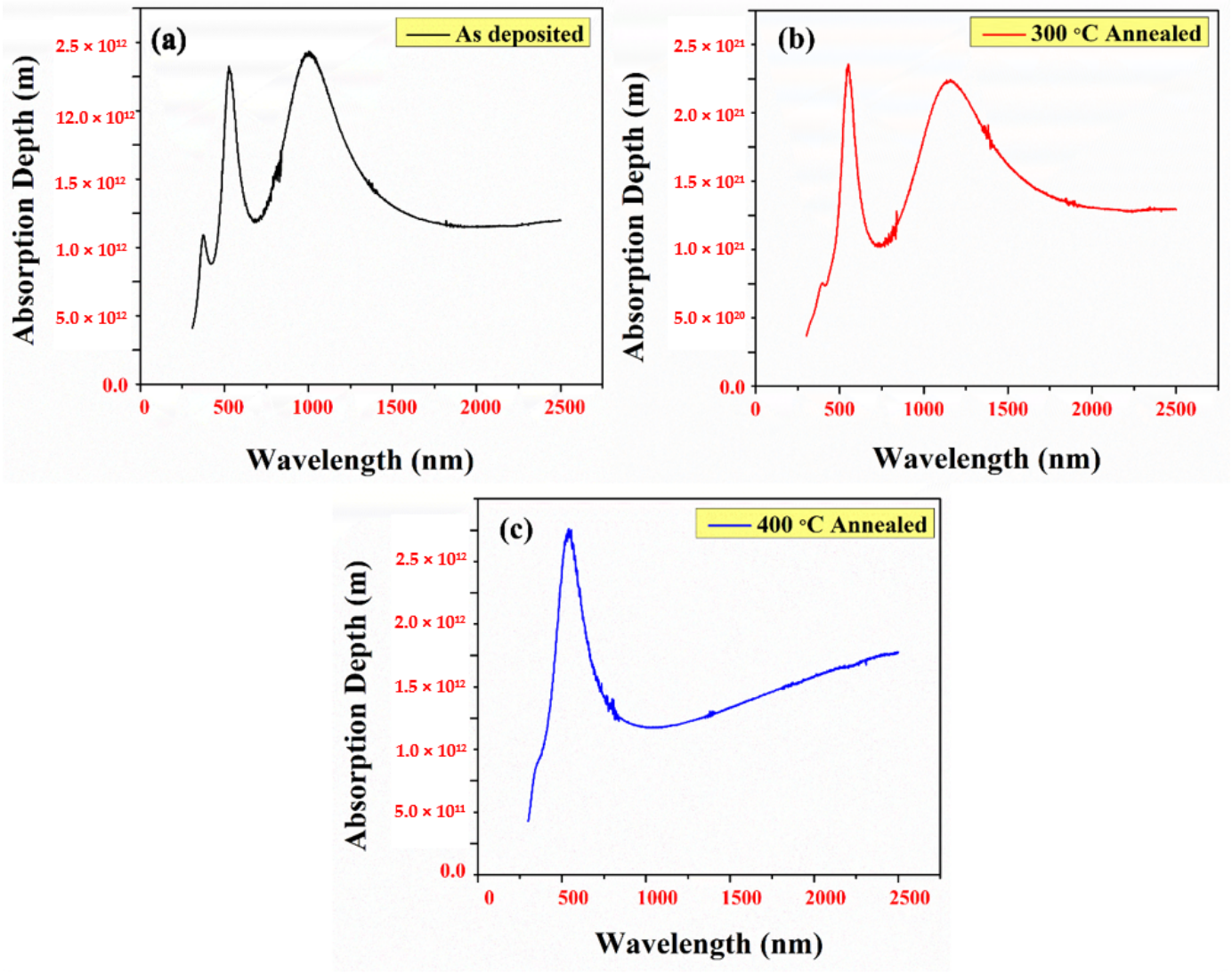

Figure 4. Absorption depth (α) vs. wavelength (nm) of multi-layered $HfO_2/V_2O_5/HfO_2$ thin films: (**a**) as-deposited; (**b**) annealed at 300 °C; and (**c**) annealed at 400 °C.

Figure 5 shows the fitted and experimental RBS spectra of the multi-layered $HfO_2/V_2O_5/HfO_2$ thin films. The spectra in Figure 5a show no impurities within the prepared films, and the thin films were composed of the desired elements, i.e., Hf, V, and O (surface/film). The presence of Ca and Si stemmed from the underlying soda–lime glass substrate.

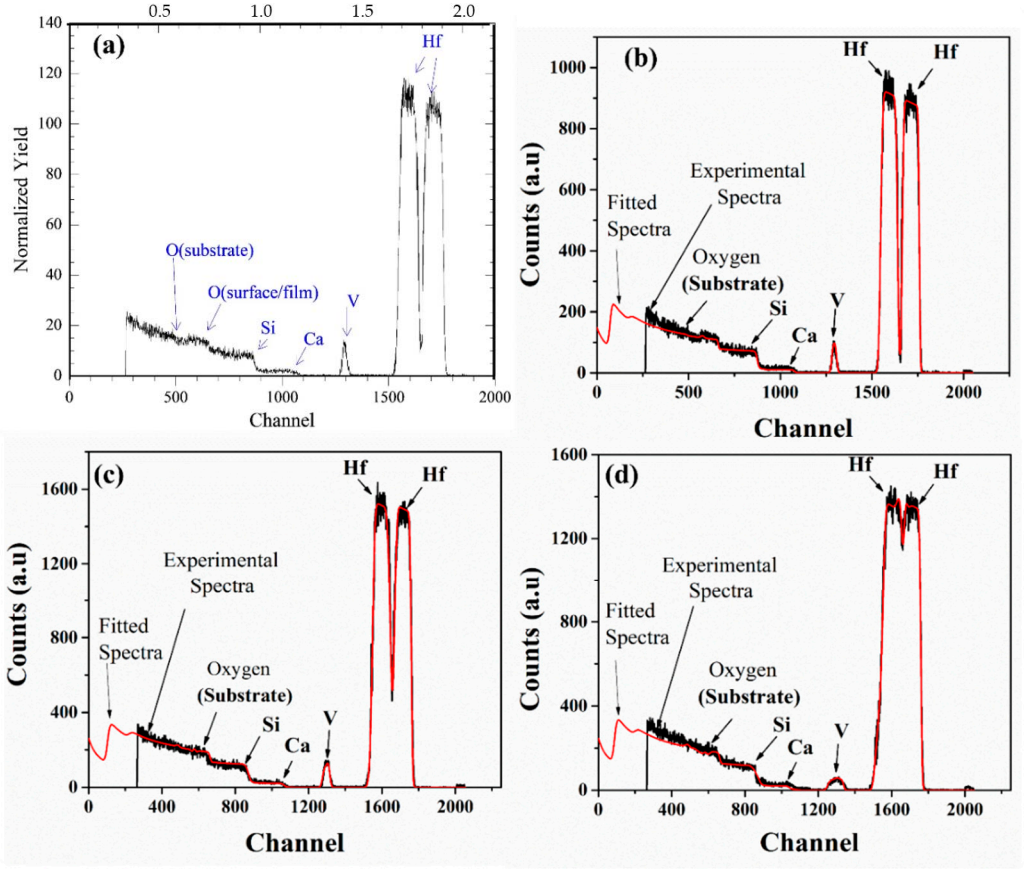

Figure 5. (**a**). Fitted and experimental RBS spectra of nanostructured multi-layered $HfO_2/V_2O_5/HfO_2$ coatings: (**b**). as-deposited; (**c**) annealed at 300 °C; and (**d**) annealed at 400 °C.

The RBS spectra in Figure 5b reveal relatively sharp peaks and a sharp interface between the layers. Moreover, two Hf peaks are present in the RBS spectra, and the dip between these two peaks confirms that Hf was coming from the two different layers (bottom and upper HfO_2 layers, as seen in Figure 1). This indicates that there was a distance between the two layers from which Hf was coming. This indicates a presence of a layer in between the two HfO_2 layers, i.e., the V_2O_5 layer. As reported [28–30], the ratio of elements was determined via in-depth profiling. In the as-deposited thin film, the calculated thickness of 104 nm was determined, agreeing with the theoretical intended value of 100 nm (Table 1). Thus, the development of the thin films was conducted with high accuracy. Moreover, the presence of Ca, Si, and substrate oxygen (O) stemming from the underlying substrate was not present in the material. This confirmed no porosity on the prepared thin films [31–34]. The sharp interface between the different layers, i.e., HfO_2 and V_2O_5, is clearly visible from the RBS spectra. As the resolution of RBS is ~7 nm, the sharp interface between the different layers is <7 nm.

After 1 h annealing at 300 °C in air, the layers started to diffuse into each other due to the thermal treatment. The dip between the two Hf peaks decreased with increased annealing temperature, indicating that the distance between the two layers (from which Hf is derived), i.e., HfO_2, was decreasing. Thus, the layers began to merge into one another, as shown in Figure 5c. Moreover, the height of the Hf and V peaks decreased as the FWHM increased. This was due to diffused interface present between the layers that arose as a result of diffusion with increased annealing temperature. Nevertheless, the total area under the curve remained the same. The in-depth profiling revealed diffused interface between the two HfO_2 layers and the V_2O_5 layer, as shown in Table 2.

Table 2. In-depth profiling of a 400 °C annealed sample's thickness and its elemental ratios.

Layer	Thickness	Hf	V	O (film)	Si	Ca	O (Substrate)
1	76 nm	0.256	0	0.743	0	0	0
2	76–85 nm	0.278	0.106	0.615	0	0	0
3	85–102 nm	0.298	0.103	0.598	0	0	0
4	102–110 nm	0	0.112	0.873	0	0	0
5	110–144 nm	0.290	0.102	0.607	0	0	0
6	144–168 nm	0.263	0.07	0.66	0	0	0
7	168–235 nm	0.244	0	0.756	0	0	0
8	235–258 nm	0.065	0	0.204	0.143	0.005	0.580
9	258–274 nm	0.036	0	0.186	0.267	0.009	0.601
10	274–4000 nm	0	0	0	0.322	0.033	0.644

The RBS spectrum (Figure 5c) shows a decrease in the dip between the two Hf peaks compared to Figure 5b. Moreover, the V peak spreads widely, confirming that the distance between the two layers from which Hf was coming, i.e., HfO_2, was decreasing, and indicating that the layers were starting to diffuse into each other (but not fully). Additionally, as the FWHM grew, the height of the Hf and V peaks decreased, confirming that there was a diffused interface present between layers that arose due to diffusion as the temperature increased. Nevertheless, the total area under the curve remained similar.

Moreover, two peaks represent Hf with different total heights of the peak. Indeed, the height of the peak indicates the position of the HfO_2 thin film in our material, i.e., the smaller peak stems from the HfO_2 adjacent to the substrate, whereas the highest peak represents the top HfO_2 thin film. This difference is related to energy loss in a scattering cross-section. The thickness of the diffused interface between HfO_2 (layers 2 and 3) and the V_2O_5 (layers 4 and, 5) showed increased in-depth profiling for materials annealed at 400 °C, as shown in Table 2. A substantial amount of V appeared in these layers, indicating that as the temperature increases, the layers will mix and a diffused interface will occur. Layers 8 and 9 also exhibited the formation of a diffused contact between the substrate and bottom HfO_2 layer.

Electrical properties were measured through a two-point probe technique and, subsequently, the resistance and conductivity were calculated using the following equations:

$$\rho = R \times t \tag{3}$$

$$\sigma = 1/\rho \tag{4}$$

where ρ (Ωcm) is the resistivity, R (Ω) is the resistance, t (nm) is the thickness, and σ ($\Omega^{-1}cm^{-1}$) is the conductivity.

The conductivity of the thin films is depicted in Figure 6. The conductivity of annealed thin films increased compared to the as-deposited ones because the conductivity of the as-deposited thin film is 0.223 $\Omega^{-1}cm^{-1}$, which is greater than the HfO_2 (1×10^{-5} $\Omega^{-1}cm^{-1}$) layer and less than the V_2O_5 (0.32 $\Omega^{-1}cm^{-1}$) layer. The change in conductivity of our thin films was due to the measured conductivity of combined layers, and each layer had a different atomic arrangement as well as an interface between each layer, which caused the conductivity of our as-deposited sample to differ from theoretical values. The other reason for lowering the conductivity of the as-deposited thin films is that the strong interface between the layers caused electron scattering and prevented electron transport, as mentioned in Table 1, which concerns RBS data. The conductivities of thin films annealed at 300 °C and 400 °C were 1.02 $\Omega^{-1}cm^{-1}$ and 1.9 $\Omega^{-1}cm^{-1}$, respectively.

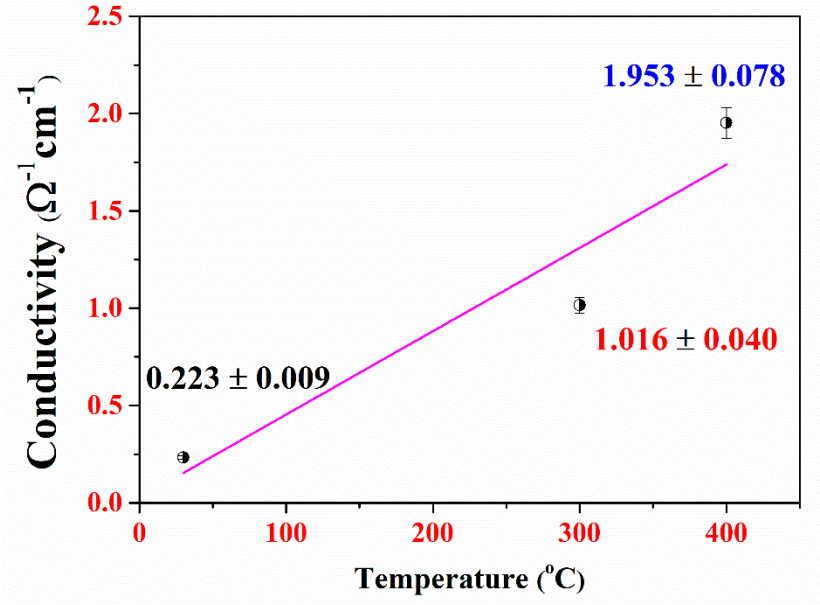

Figure 6. The plot of conductivity ($\Omega^{-1}cm^{-1}$) vs. temperature (°C) of nanostructured multi-layered $HfO_2/V_2O_5/HfO_2$ thin films.

Based on RBS, when the V_2O_5 and HfO_2 layers were heated, a diffused interface formed between them, as shown in Table 3. As a result, electron scattering was reduced in comparison to the as-deposited thin films because electrons obtained a path to flow through, which ultimately increased the conductivity. For thin films annealed at 400 °C, the highest conductivity was achieved. This was due to diffusing the HfO_2 and V_2O_5 layers into each other, causing the thickness of the diffused interface to increase, as shown in Table 3, and giving electrons a relatively smooth path to flow. Due to this, conductivity increased with increased annealing temperature.

Table 3. In-depth profiling of a 300 °C annealed sample's thickness and its elemental ratios.

Layer	Thickness	Hf	V	O (Film)	Si	Ca	O (Substrate)
1	90 nm	0.271	0	0.728	0	0	0
2	90–106 nm	0.15	0.298	0.5512	0	0	0
3	106–146 nm	0	0.123	0.877	0	0	0
4	146–163 nm	0.199	0.212	0.588	0	0	0
5	163–250 nm	0.261	0	0.738	0	0	0
6	250–265 nm	0.020	0	0.203	0.218	0.006	0.550
7	265–4000 nm	0	0	0	0.322	0.033	0.644

All in all, THM are energy-efficient thin films designed to save energy in hot climates by reflecting infrared heat and allowing only the visible part of solar radiation to pass through the films. Such thin films can potentially be used as energy-saving windows in energy-efficient buildings and greenhouse agriculture. The thin films presented herein, based on $HfO_2/V_2O_5/HfO_2$, possess all of the intrinsic properties of an efficient THM and should be considered for potential use for this application.

4. Conclusions

Fabrication via e-beam evaporation of multi-layered $HfO_2/V_2O_5/HfO_2$ thin films with a thickness of 100/60/100 nm was shown for their potential use as THM. The as-deposited and annealed thin films (at 300 °C and 400 °C in air) possess a transmittance of approximately 90%. The relatively high transmittance is due to the interface diffusion of HfO_2 and V_2O_5 layers. The optical E_{BG} of 3.28 eV and 2.17 eV was obtained for the

as-deposited HfO_2 and V_2O_5 thin films, respectively. A slight decrease in E_{BG} was observed after annealing at 300 °C (E_{BG} ~3.24 eV HfO_2; E_{BG} ~2.07 eV V_2O_5) and 400 °C (E_{BG} ~3.23 eV HfO_2; E_{BG} ~1.94 eV V_2O_5). The RBS confirmed uniform thin films with no porosity or pinholes. The qualitative analysis of Rutherford backscattering spectroscopy results shows that developed thin films were fabricated with high accuracy using electron beam evaporation because the thickness of developed layers calculated by RBS is similar to the intended thickness. The conductivities of as-deposited films, films annealed at 300 °C, and films annealed at 400 °C were 0.223 $\Omega^{-1}cm^{-1}$, 1.02 $\Omega^{-1}cm^{-1}$, and 1.9 $\Omega^{-1}cm^{-1}$, respectively. Interface diffusion is responsible for increased conductivity in annealed thin films compared to that of as-deposited ones. The intrinsic properties of the developed thin films support their use as transparent heat mirrors.

Author Contributions: Conceptualization, A.F.K.; methodology, M.M., D.A.C., M.O.D., M.B.H.; software, A.F.K.; validation, M.M., D.A.C., M.O.D., M.B.H.; formal analysis, D.A.C., M.O.D., M.B.H.; investigation D.A.C., M.O.D.; resources, A.F.K.; data curation, D.A.C., M.O.D.; writing—original draft preparation, D.A.C., M.O.D., M.B.H., M.M., A.F.K., A.S.A., M.R., A.K., T.S.; writing—review and editing, D.A.C., M.O.D., M.B.H., M.M., A.F.K., A.S.A., M.R., A.K, T.S.; visualization, A.F.K., M.M., T.S.; supervision, A.F.K.; project administration, A.F.K., M.M.; funding acquisition, A.F.K., T.S. All authors have read and agreed to the published version of the manuscript.

Funding: This research has been funded by the Scientific Research Deanship at the University of Ha'il (Saudi Arabia) through project No.RG-21 065.

Institutional Review Board Statement: Not applicable.

Informed Consent Statement: Not applicable.

Data Availability Statement: The data presented in this study are available from the corresponding author upon request.

Conflicts of Interest: The authors declare no conflict of interest. The funders had no role in the design of the study; in the collection, analyses, or interpretation of data; in the writing of the manuscript; or in the decision to publish the results.

References

1. Ramzan, M.; Rana, A.; Ahmed, E.; Wasiq, M.; Bhatti, A.; Hafeez, M.; Ali, A.; Nadeem, M. Optical characterization of hafnium oxide thin films for heat mirrors. *Mater. Sci. Semicond. Process.* **2015**, *32*, 22–30. [CrossRef]
2. Palamutcu, S. Electric energy consumption in the cotton textile processing stages. *Energy* **2010**, *35*, 2945–2952. [CrossRef]
3. Hanif, M.B.; Motola, M.; Qayyum, S.; Rauf, S.; Khalid, A.; Li, C.-J.; Li, C.-X. Recent advancements, doping strategies and the future perspective of perovskite-based Solid oxide fuel cells for energy conversion. *Chem. Eng. J.* **2022**, *428*, 132603. [CrossRef]
4. Hanif, M.B.; Rauf, S.; Motola, M.; Babar, Z.U.D.; Li, C.-J.; Li, C.-X. Recent progress of perovskite-based electrolyte materials for solid oxide fuel cells and performance optimizing strategies for energy storage applications. *Mater. Res. Bull.* **2022**, *146*, 111612. [CrossRef]
5. Babar, Z.U.D.; Hanif, M.B.; Gao, J.T.; Li, C.J.; Li, C.X. Sintering behavior of $BaCe_{0.7}Zr_{0.1}Y_{0.2}O_{3-\delta}$ electrolyte at 1150 °C with the utilization of CuO and Bi_2O_3 as sintering aids and its electrical performance. *Int. J. Hydrogen Energy* **2022**, *47*, 7403–7414. [CrossRef]
6. Thirunavukkarasu, G.K.; Bacova, J.; Monfort, O.; Dworniczek, E.; Paluch, E.; Hanif, M.B.; Rauf, S.; Motlochova, M.; Capek, J.; Hensel, K.; et al. Critical comparison of aerogel TiO_2 and P25 nanopowders: Cytotoxic properties, photocatalytic activity and photoinduced antimicrobial/antibiofilm performance. *Appl. Surf. Sci.* **2022**, *579*, 152145. [CrossRef]
7. Kamalisarvestani, M.; Saidur, R.; Mekhilef, S.; Javadi, F. Performance, materials and coating technologies of thermochromic thin films on smart windows. *Renew. Sustain. Energy Rev.* **2013**, *26*, 353–364. [CrossRef]
8. Li, S.; Xu, Q.; Zhou, Z.; Zhao, W.; Li, X.; Wen, Z.; Yao, Y.; Xu, H.; Deng, H.; Dai, N.; et al. Flexible transparent heat mirror for thermal applications. *Nanomaterials* **2020**, *10*, 2479. [CrossRef]
9. Silva, G.A. Introduction to nanotechnology and its applications to medicine. *Surg. Neurol.* **2004**, *61*, 216–220. [CrossRef]
10. Rostami, M.; Talebzadeh, N.; O'Brien, P.G. Transparent photonic crystal heat mirrors for solar thermal applications. *Energies* **2020**, *13*, 1464. [CrossRef]
11. Wiatrowski, A.; Obstarczyk, A.; Mazur, M.; Kaczmarek, D.; Wojcieszak, D. Characterization of HfO_2 optical coatings deposited by MF magnetron sputtering. *Coatings* **2019**, *9*, 106. [CrossRef]
12. Capone, S.; Leo, G.; Rella, R.; Siciliano, P.; Vasanelli, L.; Alvisi, M.; Rizzo, A. Physical characterization of hafnium oxide thin films and their application as gas sensing devices. *J. Vac. Sci. Tech. A* **1998**, *16*, 3564–3568. [CrossRef]

13. Ramzan, M.; Rana, A.; Hafeez, M.; Ahmed, E.; Bhatti, A.S.; Wasiq, M.F.; Nadeem, M.Y. Optical Analysis of Hafnium Oxide-aluminum Multilayer Structures for Transparent Heat Mirrors. *Acta Chim. Slov.* **2014**, *61*, 80–86. [PubMed]
14. Azens, A.; Granqvist, C. Electrochromic smart windows: Energy efficiency and device aspects. *J. Solid State Electrochem.* **2003**, *7*, 64–68. [CrossRef]
15. Nagabharana, R.M.; Kiran, N.; Guha, P.; Sundaravel, B.; Bhatta, U.M. Structural characterization of magnetron sputtered ZnO thin films on Si (100) using RBS, scanning and high resolution transmission electron microscopy methods. *Surf. Interfaces* **2019**, *15*, 239–243. [CrossRef]
16. Kumar, B.R.; Subba, T.R. AFM studies on surface morphology, topography and texture of nanostructured zinc aluminum oxide thin films. *Dig. J. Nanomater. Biostruct.* **2012**, *7*, 1881–1889.
17. Vasiliev, M.; Mohammad, N.; Kamal, A. Transparent heat regulation materials and coatings: Present status, challenges, and opportunity. In *Energy Saving Coating Materials*; Elsevier: Amsterdam, The Netherlands, 2020; pp. 57–82.
18. Axinte, E. Glasses as engineering materials: A review. *Mater. Des.* **2011**, *32*, 1717–1732. [CrossRef]
19. Rakshit, A.; Islam, K.; Sultana, R.; Chakraborty, S. Effect of oxygen content and crystallization temperature on the insulator-to-metal transition properties of vanadium oxide thin-films. *Vacuum* **2020**, *180*, 109633. [CrossRef]
20. Zhao, X.; Mofid, S.; Gao, T.; Tan, G.; Jelle, B.; Yin, X.; Yang, R. Durability-enhanced vanadium dioxide thermochromic film for smart windows. *Mater. Today Phys.* **2020**, *13*, 100205. [CrossRef]
21. Xia, F.; Yang, L.; Dai, B.; Yang, Z.; Xu, L.; Gao, G.; Sun, C.; Song, Z.; Ralchenko, V.; Zhu, J. Thermal transition behaviors of vanadium pentoxide film during post-deposition annealing. *Surf. Coat. Technol.* **2021**, *405*, 126637. [CrossRef]
22. Khan, A.F.; ul Abadeen, Z.; Hanif, M.B.; Saleem, M.S.; Naveed, K.; Bashir, K.; Ahmad, I. Multi-layer MgF_2/ITO coatings for electromagnetic interference shielding. *Mater. Chem. Phys.* **2021**, *272*, 125009. [CrossRef]
23. More, A.J.; Patil, R.S.; Dalavi, D.S.; Suryawanshi, M.P.; Burungale, V.V.; Kim, J.H.; Patil, P.S. Synthesis and characterization of potentiostatically electrodeposited tungsten oxide thin films for smart window application. *J. Electron. Mater.* **2017**, *46*, 974–981. [CrossRef]
24. Khmissi, H.; Mahmoud, S.A.; Akl, A.A. Investigation of thermal annealing effect on the microstructure, morphology, linear and non-linear optical properties of spray deposited nanosized V_2O_5 thin films. *Optik* **2021**, *227*, 165979. [CrossRef]
25. Dalavi, D.S.; Bhosale, A.K.; Desai, R.S.; Patil, P.S. Energy efficient electrochromic smart windows based on highly stable CeO_2-V_2O_5 optically passive counter electrode. *Mater. Today Proc.* **2021**, *43*, 2702–2706. [CrossRef]
26. Vargas, M.; Murphy, N.R.; Ramana, C.V. Structure and optical properties of nanocrystalline hafnium oxide thin films. *Opt. Mater.* **2014**, *37*, 621–628. [CrossRef]
27. Al-Kuhaili, M.F. Optical properties of hafnium oxide thin films and their application. *Opt. Mater.* **2004**, *27*, 383–387. [CrossRef]
28. Xing, S.; Zhang, N.; Song, Z.; Shen, Q.; Lin, C. Preparation of hafnium oxide thin film by electron beam evaporation of hafnium incorporating a post thermal process. *Microelectron. Eng.* **2003**, *66*, 451–456. [CrossRef]
29. Durrani, S.M.A. CO-sensing properties of hafnium oxide thin films. *Sens. Actuators B Chem.* **2007**, *120*, 700–705. [CrossRef]
30. Chris, J.; Colaux, J.L. Thin film depth profiling by ion beam analysis. *Analyst* **2016**, *141*, 5944–5985.
31. Umapathy, G.R.; Ojha, S.; Rani, K.; Thakur, M.; Mahajan, R.; Chopra, N.K.S.; Kanjilal, D. Composition profile of thin film target by Rutherford backscattering Spectrometry. In Proceedings of the 61st DAE-BRNS Symposium on Nuclear Physics, Kolkata, India, 5–9 December 2016.
32. Rocchini, M.; Chiari, M.; Pasquali, E.; Nannini, A.; Hadyńska-Klęk, K.; Sona, P.; Bazzacco, D.; Benzoni, G.; Camera, F.; Czelusniak, C.; et al. Applications of Rutherford backscattering analysis methods to nuclear physics experiments. *Nucl. Instrum. Phys. Res. Sect. B Beam Interact. Mater. At.* **2021**, *486*, 68–72. [CrossRef]
33. Luo, X.; Demkov, A.A.; Triyoso, D.; Fejes, P.; Gregory, R.; Zollner, S. Combined experimental and theoretical study of thin hafnia films. *Phys. Rev. B* **2008**, *78*, 245314. [CrossRef]
34. Bilal, U.; Ramzan, M.; Imran, M.; Naz, G.; Mukhtar, M.W.; Fahim, F.; Iqbal, H. HfO_2-based nanostructured thin films (ie, low-e coatings) with robust optical performance and energy efficiency. *J. Nanostruct. Chem.* **2022**. [CrossRef]